

Mechanisms of autogenous shrinkage of alkali-activated fly ash-slag pastes cured at ambient temperature within 24 h

Guohao Fang, Hossein Bahrami, Mingzhong Zhang*

Advanced and Innovative Materials (AIM) Group, Department of Civil, Environmental and Geomatic Engineering, University College London, London WC1E 6BT, UK

HIGHLIGHTS

- Autogenous shrinkage of AAFS pastes with various slag replacement ratios of fly ash measured.
- Autogenous shrinkage and chemical shrinkage of AAFS pastes increase with increasing slag content.
- Autogenous shrinkage of AAFS pastes in liquid stage results from chemical shrinkage.
- Autogenous shrinkage of AAFS pastes in hardening stage is not solely due to self-desiccation.
- Volume fraction of small pores of AAFS pastes decreases with increasing slag content.

ARTICLE INFO

Article history:

Received 16 December 2017

Received in revised form 19 March 2018

Accepted 20 March 2018

Keywords:

Alkali-activated cement

Shrinkage

Isothermal reaction kinetics

Microstructure

Pore size distribution

ABSTRACT

This paper aims to provide a better understanding of autogenous shrinkage of alkali-activated fly ash-slag (AAFS) pastes at very early age (<24 h). The autogenous shrinkage of AAFS pastes with 10%, 20% and 30% slag replacement ratios of fly ash is measured. The results show that increasing the slag content in AAFS pastes would accelerate the chemical reaction process and cause a higher autogenous shrinkage and chemical shrinkage. The autogenous shrinkage of AAFS pastes in the liquid stage (from 0 h to initial setting time) is caused by chemical shrinkage, which arises from the absolute volume reduction of reaction products comparing with the original volume of unreacted binder. This phenomenon is similar to that found in Portland cement (PC) systems. Nevertheless, in hardening stage (from final setting time to 24 h) the autogenous shrinkage may be not fully attributed to the self-desiccation process that occurs in PC systems. Some other reactions including the continuous reorganization and rearrangement of aluminosilicate gel structure may also contribute to the development of autogenous shrinkage. In addition, the autogenous shrinkage in early 24 h occurs mainly due to volume contraction by chemical shrinkage in fresh state, which occupies approximately 70% of total autogenous shrinkage.

© 2018 The Authors. Published by Elsevier Ltd. This is an open access article under the CC BY license (<http://creativecommons.org/licenses/by/4.0/>).

1. Introduction

Alkali-activated materials (AAM) have been studied over the past decades because of its environmental benefits and superior engineering properties, e.g., mechanical properties and chemical durability [1–3]. Based on the chemical compositions of raw materials, AAM can be divided into two sole systems, including high calcium system (e.g., alkali-activated slag (AAS)) and low calcium system (e.g., alkali-activated fly ash (AAF)) [4]. However, these two sole systems have some critical drawbacks. For instance, AAS has issues related to fresh properties such as quick setting problems [5], while AAF needs to be cured under an elevated temperature of 60–85 °C [6–8]. Therefore, it is essential to find a new AAM

system, e.g., alkali-activated fly ash-slag (AAFS) blended system, which can achieve superior engineering properties under ambient curing condition [9–17]. Nevertheless, the practical applications of AAFS remain low mainly due to the uncertain long-term durability and insufficient ability against shrinkage and micro-cracking [18,19].

Shrinkage is an important engineering property of Portland cement (PC) concrete that can affect the cracking probability and thus durability of concrete by providing easy access of water and aggressive species into the interior of concrete. Shrinkage is a broad term given to the volume reduction of concrete, which can be classified as different types including plastic shrinkage, chemical shrinkage, autogenous shrinkage, drying shrinkage and carbonation shrinkage [20]. Plastic shrinkage occurs if the water is allowed to escape from the surface of concrete during the plastic state. Chemical shrinkage results from the reduction in absolute

* Corresponding author.

E-mail address: mingzhong.zhang@ucl.ac.uk (M. Zhang).

volume of hydration products compared to the original volume of unhydrated cement. When concrete is sealed, cement hydration leads to autogenous shrinkage via reducing the internal moisture. When concrete is exposed to normal drying environmental conditions, moisture diffusion of the hardened concrete results in drying shrinkage along with carbonation shrinkage due to the reaction with carbon dioxide [20].

Similarly, shrinkage is also one of the important properties for AAM based concrete. An increasing number of studies have been conducted to investigate the shrinkage of AAM. It was found that the sole AAM systems have significantly higher autogenous shrinkage and drying shrinkage than PC systems [21–23]. It was also reported that the shrinkage of the sole systems is influenced by different factors, such as the chemical and physical properties of binder, the type and dosage of alkaline activator, and curing conditions [24–27]. Up to now, however, there are only a few available studies on shrinkage of AAFS. Deb and Nath [18] and Hojati and Radlinska [28] explored the effect of fly ash and slag proportions and the type of alkaline activator on shrinkage of AAFS mixtures (paste, mortar, and concrete) and found that increasing slag content and decreasing ratio of sodium silicate to sodium hydroxide in AAFS mixtures would result in high autogenous shrinkage and drying shrinkage. Nevertheless, the related mechanism of the shrinkage, particularly the autogenous shrinkage of AAFS is still not clear. Lee et al. [19] studied the shrinkage characteristics of AAFS pastes and mortar during the first 28 days and concluded that autogenous shrinkage of AAFS occurred due to the self-desiccation in hardened state rather than the volume contraction by chemical shrinkage in fresh state. However, this research mainly focused on the autogenous shrinkage at a relatively later age from days to weeks. There is still a lack of theoretical explanation of the autogenous shrinkage of AAFS during the first day after casting.

For PC systems, it is known that autogenous shrinkage is a consequence of chemical shrinkage at liquid stage. After hardening, autogenous shrinkage becomes less than chemical shrinkage since the volume reduction is restrained by a rigid skeleton of hydrating cement paste [20]. With the formation of skeleton microstructure, the contraction of chemical shrinkage is restrained, leading to the formation of voids. In addition, the continuing hydration causes the variation of water molecules and the empty of pores, which finally leads to the decrease in relative humidity as well as the increase in curvature of water-air menisci [29–31]. Such high curvature of menisci would increase the surface tension and impose compression on the walls of capillary pores and solid hydrates and thus induces contraction in hardened cement paste [22,32]. This phenomenon is called self-desiccation [20]. According to this theory, the small diameter of pores would increase the curvature of menisci and capillary, and thus cause higher autogenous shrinkage [33]. For AAFS systems, however, the autogenous shrinkage mechanism occurring at first 24 h after casting may be different when compared with the well-known self-desiccation process due to the total different chemical reaction process. The alkaline reaction of AAFS is an extremely complex process, which consists of two basic reaction processes of sole AAM systems (i.e., AAF and AAS). During this process, two main reaction products (i.e., N-A-S-H gel from AAF system and C-A-S-H gel from AAS system) do not develop separately, but they undergo structural and compositional change [34,35]. Therefore, it is necessary and vital to explore autogenous shrinkage immediately after casting in order to fully understand the mechanisms associated with autogenous shrinkage of AAFS pastes.

The main purpose of this study is to provide a better understanding of early-age autogenous shrinkage of AAFS pastes. The autogenous shrinkage and chemical shrinkage of AAFS pastes with slag content as 10%, 20% and 30% of the total binder during first 24 h after casting were measured. A series of tests were conducted to

investigate the mechanisms of early-age shrinkage of AAFS pastes. The workability was measured by flow table test. The early-age reaction and setting process was monitored through isothermal conduction calorimetry (ICC) and Vicat setting time test, respectively. In addition, the internal relative humidity (RH) was measured by humidity data logger. Furthermore, the phases composition and pore structure were characterized by X-ray diffraction (XRD) and mercury intrusion porosimetry (MIP), respectively.

2. Experimental program

2.1. Raw materials

Class F fly ash (FA) and ground granulated blast-furnace slag (GGBS) were used in this study. The chemical compositions of FA and GGBS are shown in Table 1. The particle size distribution curves are plotted in Fig. 1, with a volume-based average particle size of 14.77 μm for GGBS (Fig. 1a) and 26.81 μm for FA (Fig. 1b). The alkaline activator was prepared by mixing sodium hydroxide (>98% purity) with distilled water and sodium silicate solution. The concentration of sodium hydroxide (SH) was 10 M for all mixtures. The $\text{SiO}_2/\text{Na}_2\text{O}$ molar ratio of the sodium silicate (SS) was 2.0 with chemical composition of 26.42 wt% SiO_2 , 13.65 wt% Na_2O and 53.93 wt% H_2O . The alkali modulus (i.e., the mass ratio of SiO_2 to Na_2O) in the alkali solution was 1.12. Since the polycarboxylate-based superplasticizers (SPs) not only have a negligible effect on the reaction kinetics of AAFS but also have a significant effect on the workability [36], it was used to improve the workability of AAFS paste in this work. The properties of SPs are given in Table 2.

2.2. Mixture proportions

The AAFS pastes with three different GGBS replacement ratios for FA were designed and tested in this work. The mixture proportions of AAFS paste are given in Table 3 and denoted with specific codes. The label 'FS' represents AAFS paste, while the number, '10', '20', or '30', stands for the percentage of GGBS replacement for FA by weight. The ratio of alkaline activator to binder by weight (AL/B) was 0.4. The mass ratio of sodium silicate to sodium hydroxide (SS/SH) was 2.0. In addition, the mass ratio of SPs to binder (B) was 0.01.

2.3. Testing methods

Herein, a non-contact testing method was applied to measure the autogenous shrinkage occurring immediately after mixing the AAFS paste and continuing for the first 24 h. Moreover, a series of tests were conducted to investigate the chemical and physical phenomena causing the early-age autogenous shrinkage.

2.3.1. Autogenous shrinkage test

Early-age autogenous shrinkage can be determined by volumetric or linear measurements. Volumetric measurements monitor the volume changes of paste or mortar specimens at a constant temperature, while linear measurements can be used to evaluate the linear dimension change of paste, mortar, or concrete specimens cast in a rigid slab mould and recorded by sensors at one end or both ends of the specimens. Linear measurements can reflect the actual material behaviour as compared with volumetric measurements because the effects of other influencing factors such as thermal dilation and bleeding can be conducted in the slab test [37]. According to the sensors used in the test the linear measurements can be classified into contact and non-contact methods. Linear Variable Differential Transformer sensors (LVDTs) are commonly

Table 1
Chemical compositions (wt.%) of FA and GGBS.

Oxide	SiO ₂	Al ₂ O ₃	CaO	MgO	K ₂ O	Fe ₂ O ₃	TiO ₂	Na ₂ O	SO ₃
FA	53.24	26.42	3.65	9.55	2.57	1.65	0.86	0.76	0.56
GGBS	36.77	13.56	37.60	7.45	0.55	0.41	0.79	0.25	1.82

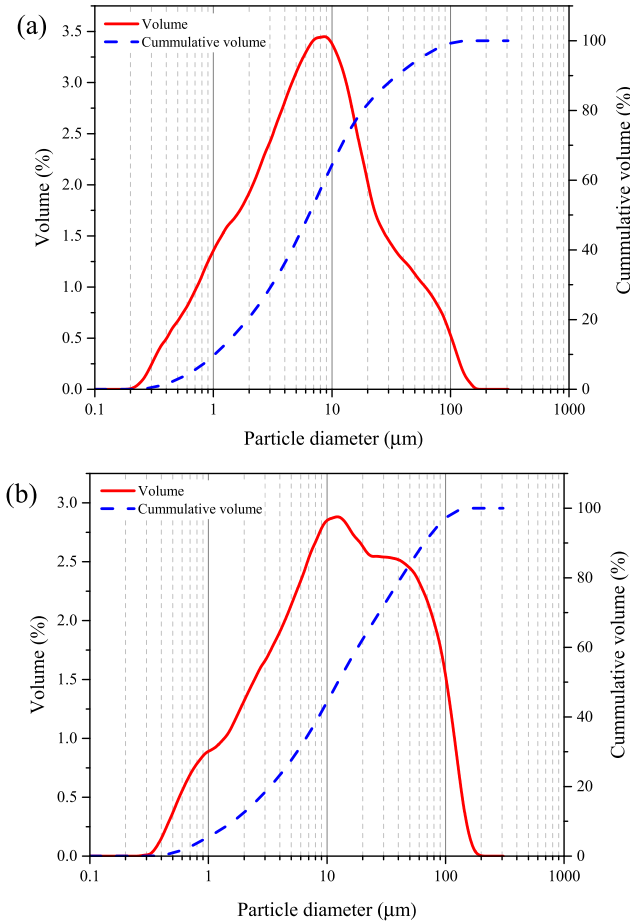


Fig. 1. Particle size distribution of: (a) GGBS; and (b) FA.

Table 2
Properties of superplasticizers.

Specific gravity (25 °C)	pH (25 °C)	Content of chloride ion (%)	Content of alkaline (%)
1.08	4–5	≤ 0.1	≤ 0.4

installed at the centre of the specimen to monitor the autogenous shrinkage [38]. However, this contact method can only be used to measure the linear dimension change of specimens after the setting time. In addition, the installed sensors may damage materials at early age and produce relative displacement during the fluid-solid transition happening around setting. In comparison, the non-contact method with laser displacement sensors is more suitable to determine the initiation point of autogenous shrinkage [39]. Moreover, this non-contact method can provide a stable and accurate result. Therefore, a non-contact method with laser displacement sensors was used in this study to monitor the early-age autogenous shrinkage of AAFS pastes after casting.

The specimen setup for autogenous shrinkage measurement is shown in Fig. 2a, which consists of two elements: 1) a PVC mould with a sealed cover, whose inner size is 70 × 70 × 70 mm; and 2)

Table 3
Mixture proportions of the AAFS pastes.

Mixtures	AL/B	FA/GGBS	SS/SH	SPs/B
FS10	0.4	90/10	2.0	0.01
FS20	0.4	80/20	2.0	0.01
FS30	0.4	70/30	2.0	0.01

an envelope formed by two PVC plates (i.e., reflecting plates) and a plastic sheet. Oil was spread between the plastic sheet and the mould to limit the friction between paste specimen and mould. The freshly mixed AAFS paste was cast into the envelope positioned in the mould. The mould was then sealed by a plastic sheet and covered by a thick PVC plate to limit the water evaporation of paste. After that, the mould was placed in the shrinkage testing chamber with a constant temperature of 20 °C and a relative humidity of 40%. When the paste specimen shrinks, the reflecting plates were dragged along by the paste in the horizontal direction. A laser sensor was then used to detect the reflecting plate's displacement, from which the horizontal deformation of specimen (i.e., autogenous shrinkage) can be calculated (as shown in Fig. 2b). The trials indicated that the displacement of two plates is almost the same. Thus, only one side's displacement was measured and used to calculate the whole horizontal deformation. The data of shrinkage were logged on a computer at 0.2 s interval for a period of 24 h. To ensure the reproducibility, three duplicate samples were prepared and measured to obtain the mean value of autogenous shrinkage.

2.3.2. Chemical shrinkage test

Chemical shrinkage tests were conducted using a volumetric method according to ASTM-12 [40]. The experimental setup is shown in Fig. 3. According to ASTM C1608-12, chemical shrinkage was calculated as the measured weight of absorbed water per gram of solid phase in binder in the paste specimen. Here, the changes of water level were measured at 10-min intervals for a period of 24 h. In addition, the data reading started at 60 min after mixing in order to eliminate the effect of testing device. Thus, the chemical shrinkage of AAFS paste at time t can be expressed as:

$$CS(t) = \frac{h(t) - h(60 \text{ min})}{M_s} \quad (1)$$

where $CS(t)$ is the chemical shrinkage at time t (mL/g), $h(t)$ is the water level in capillary tube at time t (mL), $h(60 \text{ min})$ is the water level in capillary tube at 60 min (mL), and M_s is the mass of solid phase in binder (g).

2.3.3. Workability test

The workability of AAFS paste was investigated using flow table test according to ASTM C230-14, in which the diameter of the paste spread in two directions at right angles was measured to calculate the flow value [41]. The flow value was calculated using Eq. (2).

$$F = \frac{D_1 + D_2 - D_i}{D_i} \times 100 \quad (2)$$

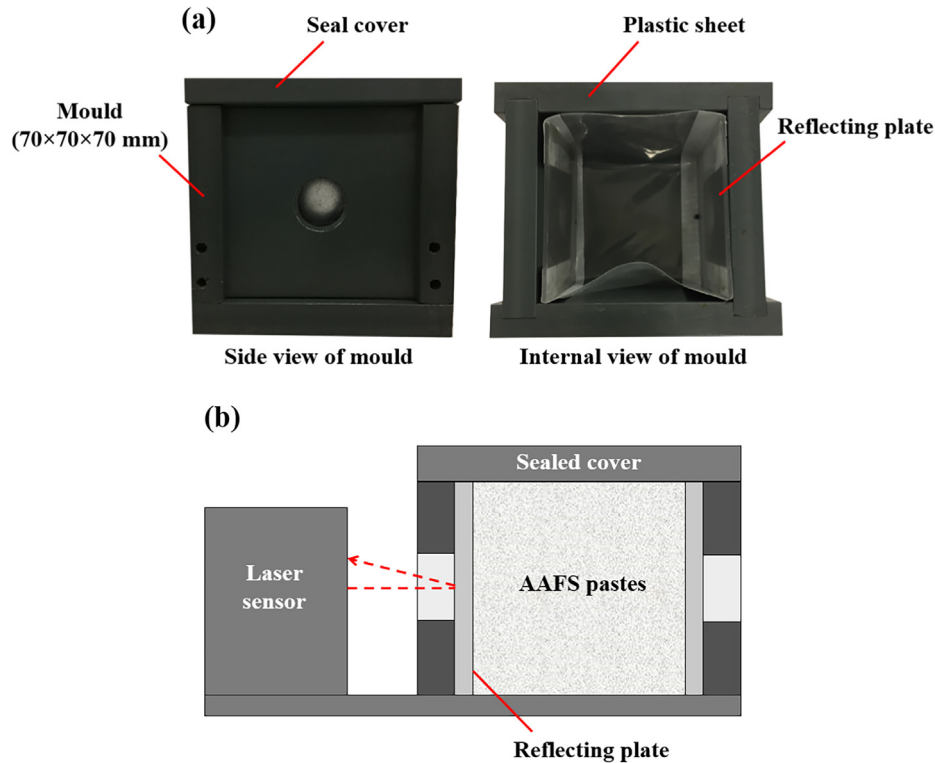


Fig. 2. (a) Autogenous shrinkage measurement mould and (b) schematic section view of autogenous shrinkage measurement.

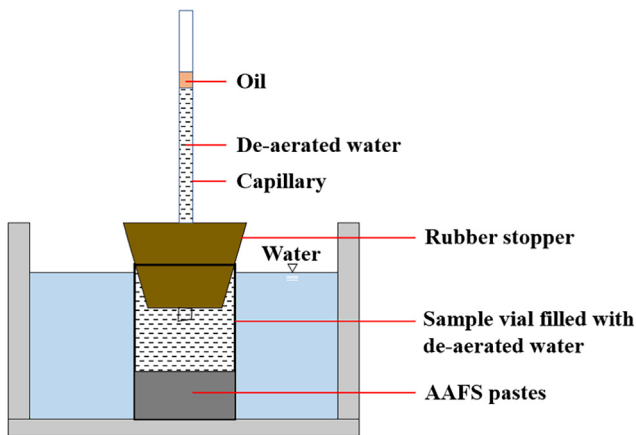


Fig. 3. Chemical shrinkage measurement setup.

where F is the flow value of AAFS paste (%), D_1 is the diameter of the paste spread in the first direction (mm), D_2 is the diameter of the paste spread in the second direction (mm), and D_i is the original inside base diameter (i.e. 100 mm).

2.3.4. Setting time test

The initial and final setting time of AAFS paste was determined by the Vicat setting test according to ASTM C191-13 [42]. The test was conducted at a controlled room temperature of 20 °C. A Vicat needle was used to measure the change of penetration depth as the structure formation can result in a reduction in the extent of penetration into the specimen. The penetration depth is the vertical distance between the initial position of Vicat needle before dropping and the final position of Vicat needle after dropping inside the paste. Accordingly, the change of penetration depth is defined as the difference between the penetration depth at first drop and

that at later drop. Here, after first drop, the penetration depth is set as the initial point. Based on this point, the change of penetration depth can be calculated. In this case, the maximum change of penetration depth will be 36 mm when the paste reaches its final setting since the height of testing mould used is set constantly as 36 mm. Thus, the initial setting time and final setting time are defined as the time elapsed between the initial contact of binder and water and the time when the change of penetration depth is measured to be 25 mm and 36 mm, respectively. The data of setting help us to study early structure formation and development of AAFS pastes.

2.3.5. Isothermal calorimetry test

The reaction of AAFS paste at early 24 h was determined at 20 °C with an isothermal calorimetry (TAM Air model, TA Instruments, USA). According to the used AL/B ratio of 0.4, 4 g of binder with different FA/GGBS ratios was mixed with 1.6 g of activator and 0.04 g of SPs in a plastic vial. Once mixed, the vial was immediately placed into the calorimeter. The data of isothermal calorimetry test contributes to investigating the early-age chemical reaction of AAFS pastes.

2.3.6. Internal relative humidity test

The internal RH of AAFS pastes at early 24 h was measured using humidity data logger (Onset HOBO UX100-003, MicroDAQ-com, Ltd, USA). As shown in Fig. 4, a hollow cylindrical filter with size of 40 × 100 mm was placed in the cylindrical mould with size of 100 × 150 mm to form a cylindrical hole where the humidity data logger was placed. The pastes were then placed and consolidated around the filter. After that, the mould was covered by a thick PVC plate and sealed by plastic wrap to limit the water evaporation. Finally, the samples were placed in a testing chamber with a constant temperature of 20 °C and a RH of 40%. The RH in the AAFS pastes sample was recorded every 10 s for 24 h.

2.3.7. Microstructure characterisation

After autogenous shrinkage test, the AAFS samples were crushed by a universal testing machine. The fracture pieces inside the AAFS samples were chosen for the microstructure tests. Before microstructure test, the specimens were stored in acetone for 3 days to stop the chemical reaction and then placed in a vacuum dryer to reach a constant weight.

The phases composition of AAFS paste was detected with the help of XRD (D8 ADVANCE, BRUKER, Germany), which used $\text{CuK}\alpha$ X-ray ($\lambda = 1.5418 \text{ \AA}$) and 2θ configuration in the range of 7° – 70° with a step size of 0.01° . Here, the powder specimens for the XRD test were prepared by mechanical grinding. The pore structure of AAFS pastes was determined using MIP (AutoPore IV 9500, Micromeritics Instrument Ltd, USA). According to the applied pressure, the pore diameter varying from $0.001 \mu\text{m}$ to $1000 \mu\text{m}$ can be measured with MIP [21]. The pressure applied for MIP test was in the range from 0 to 414 MPa. The surface tension of mercury used here is 0.485 N/m , and the contact angle between the mercury and the pore surface is 130° based on previous studies [43,44]. The porosity and pore structure can be obtained in accordance with a previous study [43].

3. Results

3.1. Autogenous shrinkage

Fig. 5a shows the autogenous shrinkage of AAFS pastes with three different amounts of slag at first 24 h after casting. It can be found that the development of autogenous shrinkage follows the similar trends but different magnitudes for all AAFS pastes. The ultimate autogenous shrinkage is recorded between $1271 \mu\epsilon$ and $1740 \mu\epsilon$ with increasing slag replacement level from 10% to 30%. According to previous research [45], increasing slag proportion in AAFS pastes can densify the microstructure of reaction products due to the difference of chemical composition. The densification of microstructure may increase the capillary pressure and thus increase the autogenous shrinkage [28]. In addition, it is

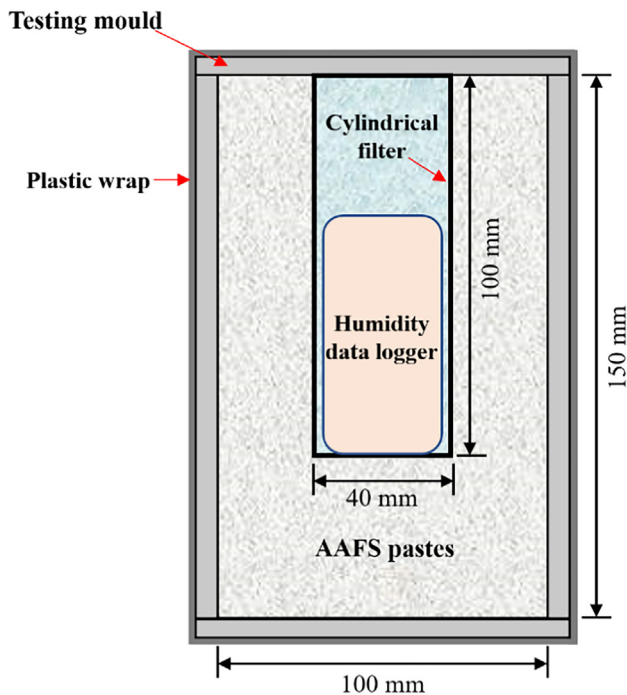


Fig. 4. Internal relative humidity measurement setup.

observed that the effect of slag at 30% replacement level on the increase of autogenous shrinkage appears to be more pronounced, in which the increasing percentage of FS30 (36.91%) is higher than that of FS20 (14.61%) as compared to FS10.

The kinetics of autogenous shrinkage of AAFS pastes is shown in Fig. 5b. It can be found that the highest autogenous shrinkage rate of FS30 ($942 \mu\epsilon/\text{h}$) and FS20 ($696 \mu\epsilon/\text{h}$) occurs at 1 h after casting. Nevertheless, the highest shrinkage rate of FS10 ($201 \mu\epsilon/\text{h}$) occurs after 2 h, which is lower than those of other two samples and tends to be delayed. It indicates that the kinetics of autogenous shrinkage of AAFS pastes are significantly dependent on the slag content.

3.2. Chemical shrinkage

Fig. 6 shows the chemical shrinkage of AAFS pastes with different slag content. It can be observed that the chemical shrinkage increases with the increase of slag content. As the slag content increases from 10% to 30%, the ultimate chemical shrinkage increases from 0.018 mL/g to 0.021 mL/g . It is indicated that the increase of slag content in AAFS pastes would accelerate the alkali-reaction process and result in a higher level of volume reduction of reaction products comparing with the original volume of unreacted binder. In addition, it is also found that the effect of slag at 20% replacement level appears to be more pronounced.

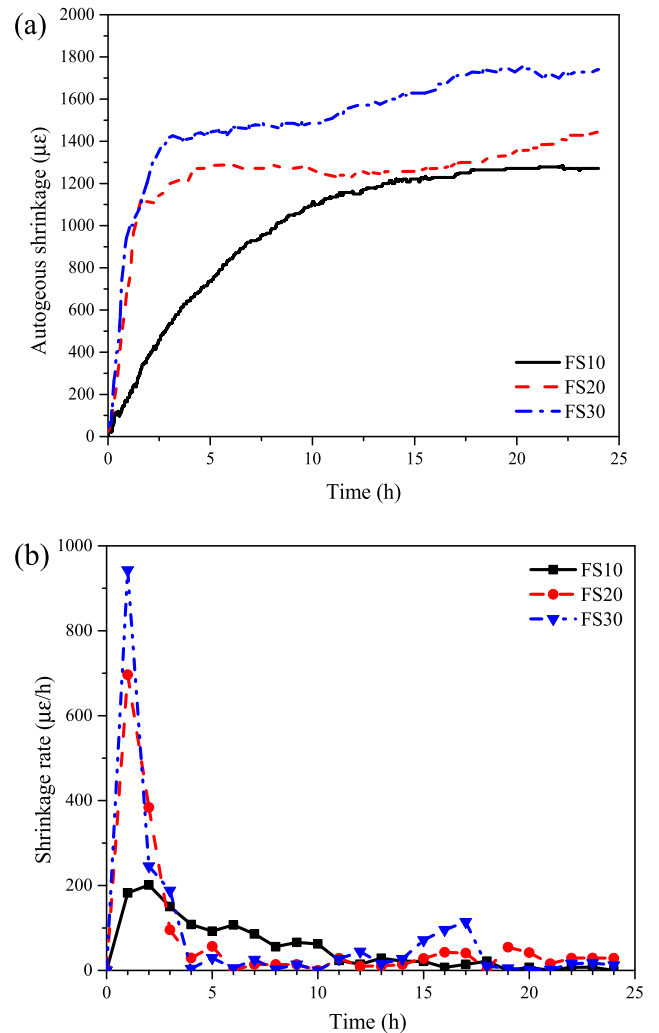


Fig. 5. (a) Autogenous shrinkage and (b) shrinkage kinetics of AAFS pastes with different slag content.

The ultimate chemical shrinkage of FS20 and FS30 is increased by 13.67% and 18.15% as compared to that of FS10, respectively. However, according to previous research [28], the higher slag content would result in a lower chemical shrinkage, which is inconsistent with the finding of this work. This can be attributed to the different molar of alkali activator used in the mixtures.

3.3. Workability

Fig. 7 shows the flow value of AAFS pastes with different amounts of slag. It can be seen that the flow value decreases with the increase of slag content. When the slag replacement level increases from 10% to 30% the flow value decreases from 137.5% to 123.5%, which indicates that the increase in slag content of the mixture would lead to an increase in the viscous degree of AAFS pastes and thus reduce the workability. Moreover, when a flow value of 120% and over is achieved, the AAFS pastes can be compact well on a vibrating table. Thus, all the AAFS pastes can be regarded as highly workable pastes and the tested AAFS pastes can fulfil the requirement of workability.

3.4. Setting time

The change of penetration depth of AAFS pastes obtained from Vicat tests is shown in Fig. 8, in which initial setting time and final setting time are indicated according to ASTM C191-13 [42]. The fluid-solid transition of AAFS pastes that happens around setting is strongly affected by the slag content of mixtures. The transition time between initial and final setting decreases from 2.09 h to 0.22 h with the increase of slag content from 10% to 30%. In addition, it can be found that increasing the slag content of mixtures would accelerate the setting of AAFS pastes. The initial setting time of pastes decreases from 6.24 h to 2.11 h and the final setting decreases from 8.33 h to 2.33 h when the slag content is increased from 10% to 30%. The addition of slag would contribute to the formation of C-A-S-H gel, which coexists with N-A-S-H gel [9]. In addition, the higher slag content may lead to more calcium releasing from the dissolution of slag and thus more C-A-S-H gel formation [35]. It was also reported that the hardened process is initiated by the precipitation of C-A-S-H gel, and rapid hardening is attributed to the accelerated alkali-reaction [46]. Thus, it suggests that the accelerated formation of C-A-S-H gel may shorten the setting time of AAFS pastes.

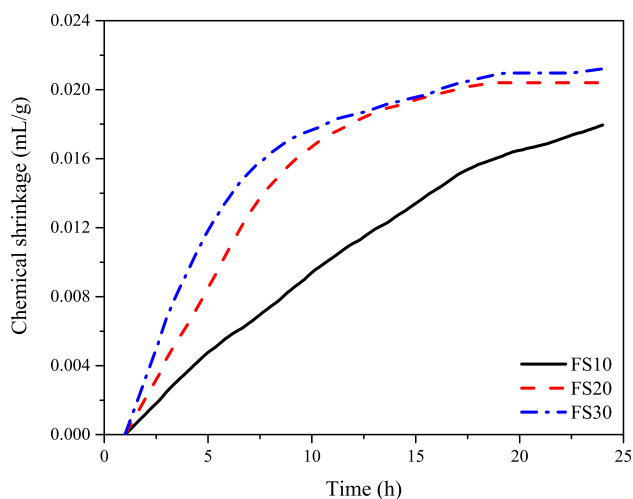


Fig. 6. Chemical shrinkage of AAFS pastes with different slag content.

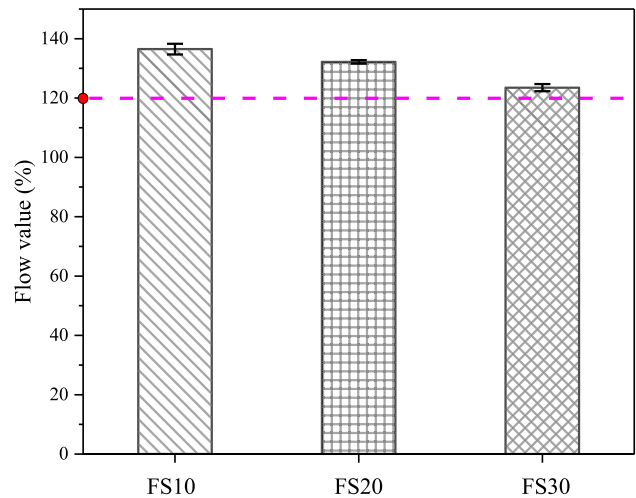


Fig. 7. Flow value of AAFS pastes with different slag content.

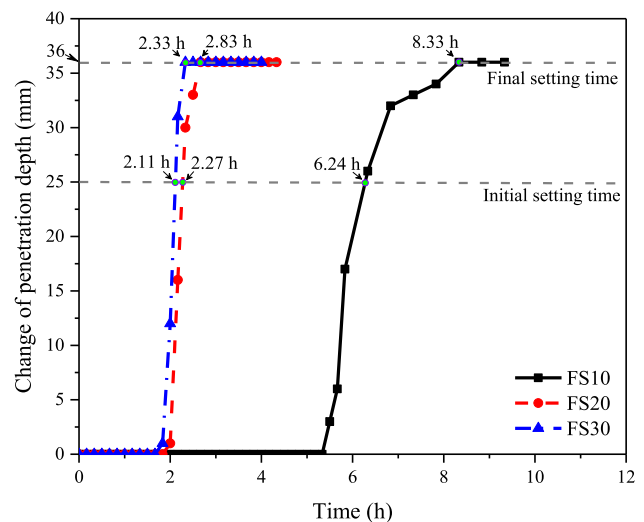


Fig. 8. Setting time of AAFS pastes with different slag content.

3.5. Isothermal reaction kinetics

Fig. 9a shows the heat evolution of AAFS pastes with different slag content within first 24 h. Two peaks can be found in the calorimetric curves, which correspond to the early dissolution of fly ash/slag particles and the later acceleration of the formation of reaction products, respectively [47]. The first initial peak can be attributed to the early stage dissolution of fly ash/slag particles and coagulation of the resulting dissolved silicate and aluminate species [48]. The second peak can be attributed to the formation of alkali aluminosilicate gels, i.e., N-A-S-H and C-A-S-H gels, as a result of condensation reaction between silicate and aluminate species and silicate present in alkaline activator [47,48]. The peak valley in the heat release curve between the first dissolution peak and the second accelerated peak is called induction period, which is related to the fluid–solid transition time (initial to final setting time). The shape of heat release curves for AAFS pastes is similar to each other even though the magnitudes and temporal occurrences are different. The induction period of AAFS pastes with higher slag content (FS20 and FS30) is found to be shorter than that of pastes with low slag content (FS10), which is corresponding to the fluid–solid transition time as shown in Fig. 8. Additionally, the accelerated peaks for pastes with higher slag content are steeper and larger.

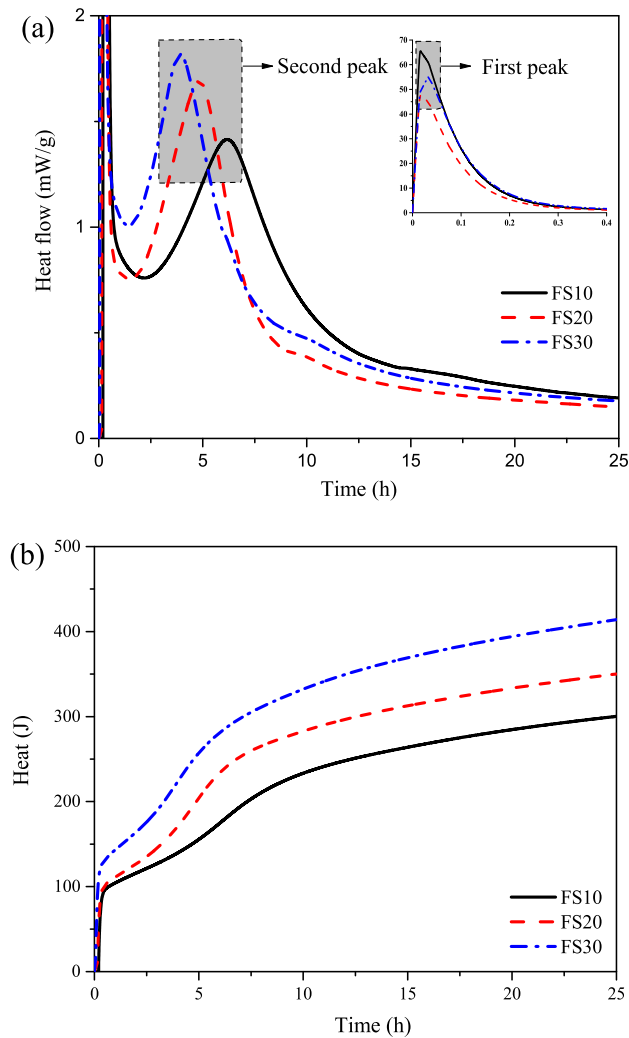


Fig. 9. (a) Heat flow and (b) cumulative heat of AAFS pastes with different slag content.

This is due to the acceleration of initial alkali-reaction facilitated by the high amounts of slag, which is corroborated by the faster setting as shown in Fig. 8. The calorimetric values in the later age show little changes because the further reaction process is controlled by diffusion.

Fig. 9b presents the cumulative heat release of AAFS pastes within 24 h reaction. The initial rising portion corresponds to the dissolution of raw materials and the second rising portion is associated with the formation of reaction products. The AAFS pastes with higher amounts of slag have a higher total cumulative heat release until 24 h. This is because a higher slag content contributes to accelerating the formation of reaction products such as C-A-S-H gels [35].

3.6. Internal relative humidity

The internal RH evolution of AAFS pastes is shown in Fig. 10. A similar developing trend of internal RH can be found for all AAFS pastes. In the first 1–2 h, there is a fast increase of the internal RH for AAFS pastes followed by a gradual increase to about 85% with time. Afterwards, the internal RH of AAFS pastes almost remains constant and would not decrease during the early-age autogenous shrinkage process, which is different comparing with the phenomenon found in PC system.

3.7. Reaction products

Fig. 11 shows the XRD pattern of AAFS pastes with different slag content. A broad hump around 26° can be found, which indicates that AAFS pastes consist of a high content of amorphous phases [19]. The peaks representing mullite ($\text{Al}_6\text{Si}_2\text{O}_{13}$) and quartz (SiO_2) can be observed in all mixtures due to the unreacted fly ash in the AAFS samples. In addition, a peak at approximately $29\text{--}30^\circ$ in 2θ can be related to poorly crystalline C-A-S-H gel according to previous XRD studies of AAFS [35]. Furthermore, a larger diffuse peak at $20\text{--}25^\circ$ in 2θ was found in FS10 as compared to FS20 and FS30 because of the formation of aluminosilicate gel [35]. It is indicated that the C-A-S-H gel would be generated along with the N-A-S-H gel in AAFS pastes [49].

3.8. Pore structure

Fig. 12 shows the pore size distribution of AAFS pastes with different slag content. As the shrinkage stress induced by capillary pressure is mainly dependent on the size and volume fraction of small pores [33], the special attention in this study is given to the variation of small pores, in particular the pores with a diameter in the range of 2–50 nm [50]. However, only pores bigger than 3.1 nm can be derived from MIP test. Thus, the fraction volume of pores larger than 3.1 nm but smaller than 50 nm is considered to estimate the variation of small pores in different AAFS pastes. The MIP results shown in Fig. 12 reveal that FS10 has the largest volume fraction of small pores (31.79%), followed by FS20 (13.64%) and FS30 (9.60%). It seems that FS10 is easier to create capillary stress during localized drying and thus cause self-desiccation.

4. Discussion

According to the stiffness of pastes, the early-age autogenous shrinkage can be divided into three stages, including liquid stage (0h-initial setting time), transition stage (initial-final setting time) and hardened stage (final setting time-24 h) [37]. Thus, in order to make a comparison between cement pastes and AAFS pastes, the mechanisms of early-age autogenous shrinkage of AAFS pastes would be discussed based on these three stages.

Fig. 13 shows the autogenous shrinkage of AAFS pastes as a function of chemical shrinkage. For AAFS pastes, a positive correla-

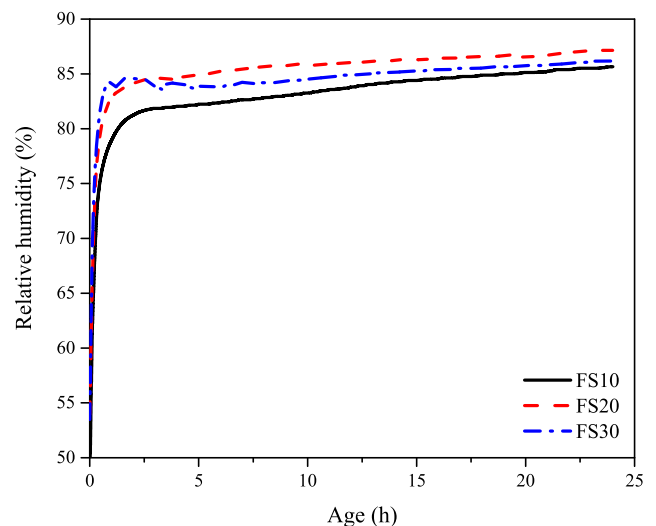


Fig. 10. Internal RH evolution of AAFS pastes.

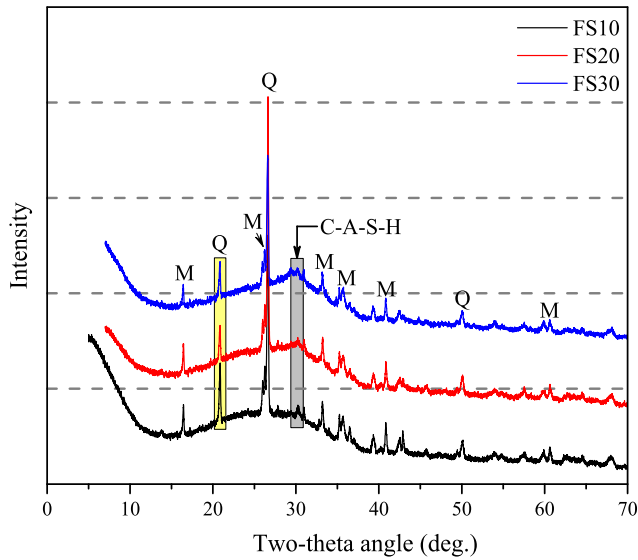


Fig. 11. XRD patterns of AAFS pastes with different slag content (Q = quartz (SiO_2 , PDF No. 89-1961), M = mullite ($\text{Al}_6\text{Si}_2\text{O}_{13}$, PDF No. 89-2644)).

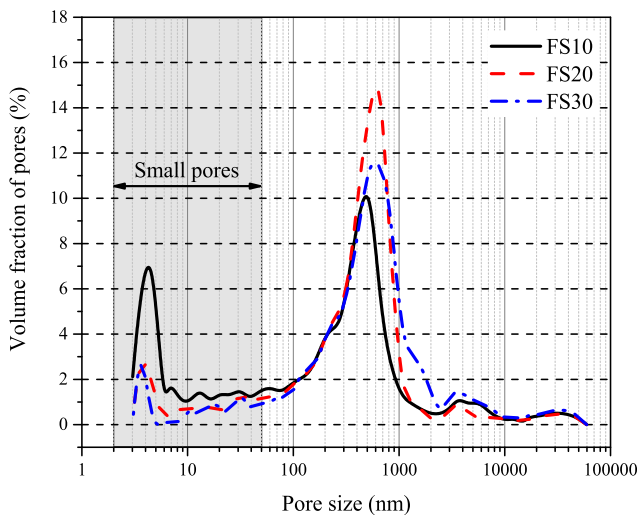


Fig. 12. Pore size distribution of AAFS pastes with different slag content.

tion between autogenous shrinkage and chemical shrinkage can be found in liquid stage, which is similar to the correlation existing in PC systems [51]. In transition stage (i.e., initial-final setting time), the curves become relatively flatter, which means the positive correlation tends to be weaker. Finally, a long-dormant plateau can be observed during the hardened stage, where the positive correlation between autogenous shrinkage and chemical shrinkage almost does not exist. In hardened stage, the autogenous shrinkage tends to be stable even though the chemical shrinkage continues to increase significantly. This is mainly because of the skeleton formation in this stage. Based on the discussion above, it can be concluded that the autogenous shrinkage of AAFS in liquid stage is mainly attributed to chemical shrinkage, which arises from the absolute volume reduction of reaction products comparing with the original volume of unreacted binder. This phenomenon is consistent with that found in PC systems. However, it should be noted that the chemical reaction occurred in AAFS pastes is different from that in PC systems. Thus, it is essential to make further discussions about the relationship between autogenous shrinkage and chemical shrinkage in liquid stage.

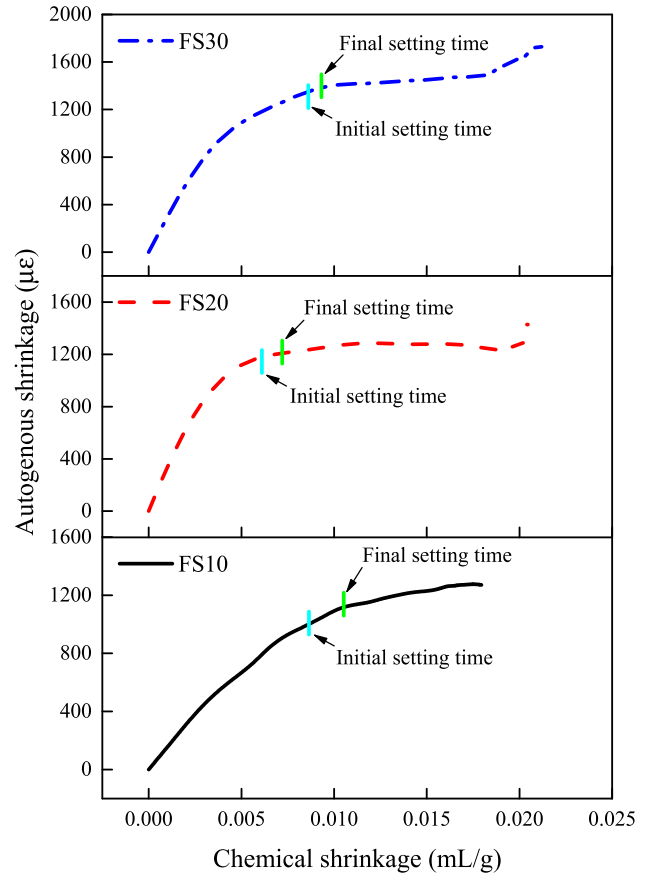


Fig. 13. Autogenous shrinkage of AAFS pastes against chemical shrinkage.

It is known that chemical shrinkage has a strong relationship with chemical reaction and it is directly proportional to the degree of hydration [52]. Thus, the relationship between autogenous shrinkage and degree of hydration can be used to further verify the correlation between autogenous shrinkage and chemical shrinkage. As seen in Fig. 14, a positive correlation between autogenous shrinkage and cumulative heat can be clearly identified in liquid stage. This further verifies that the volume contraction by chemical shrinkage plays a dominant role in the development of autogenous shrinkage in liquid stage. However, the positive relationship becomes weak in hardened stage, which indicates that the contraction of chemical shrinkage may be not the main contributor for autogenous shrinkage in this stage.

In order to study the autogenous shrinkage mechanism of AAFS pastes in hardened stage, it is necessary to analyse the pore structure. The MIP results (see Fig. 12) reveal that FS10 exhibits the largest volume fraction of pores smaller than 50 nm (31.79%), followed by FS20 (13.64%) and FS30 (9.60%). A higher volume of small pores is expected to have a larger autogenous shrinkage due to the higher self-desiccation resulting from a decrease of internal RH of AAFS pastes. Therefore, FS10 is expected to cause the largest stress on the solid, corresponding to the largest autogenous shrinkage, while FS30 with the smallest volume fraction of small pores is expected to have lowest stress, corresponding to the lowest drying shrinkage. However, AAFS samples with lower volume fractions of small pores, i.e., FS20 and FS30, exhibit a higher autogenous shrinkage as shown in Fig. 5a. Moreover, it is found that the internal RH evolution of different AAFS pastes is almost the same, where the internal RH increases to about 85% within 2 h and then becomes stable until 24 h (see Fig. 10). This implies that the autogenous shrinkage mechanism of AAFS pastes

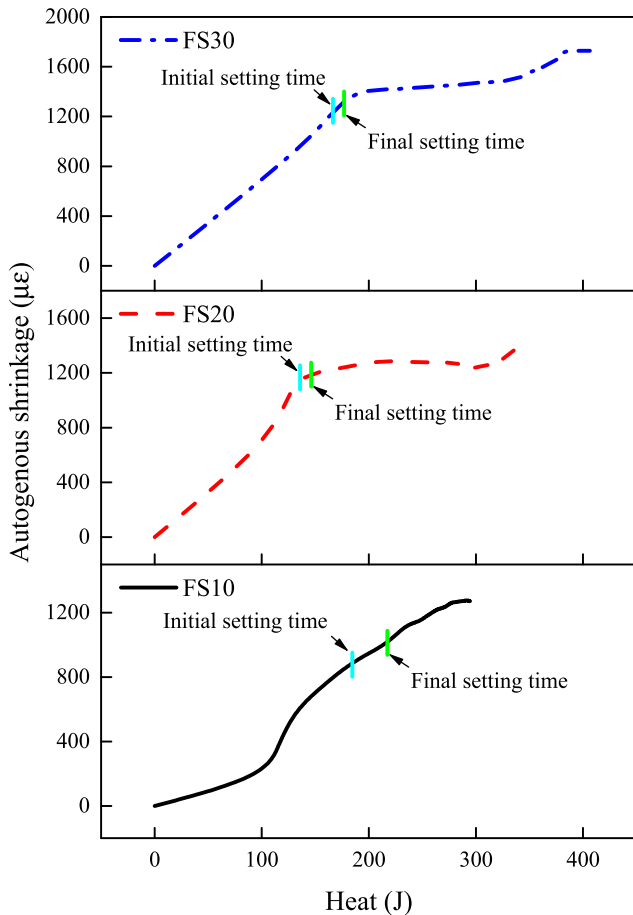


Fig. 14. Autogenous shrinkage of AAFS pastes against cumulative heat.

in hardened stage may be not fully attributed to self-desiccation, which occurs in PC systems. There may be some other reaction mechanisms contributing to the autogenous shrinkage of AAFS pastes.

In fact, the chemical reaction process of AAFS pastes is similar to the sol-gel process, in which the fine colloidal particles (the sol) would connect together to form a continuous solid phase (the gel) [53,54]. The T-O-T bonds (T: Si or Al) in fly ash particles and Ca-O and Si-O bonds in slag particles would be resolved and connected again to form new bonds in solid products during the alkaline activation process [55]. Here, the morphology of solid products depends on the degree of reversibility during the condensation process [33]. If the condensation process is nearly irreversible, a space-filling gel would form and eventually link together into a continuous gel [56]. If the condensation rate is slightly higher than the bond breaking, the products would grow along with adding new monomers [33]. In this case, the products would restructure and reorganize themselves into a more stable and denser state. In AAFS pastes, the reaction process generally occurs under conditions intermediate between the reversible and irreversible cases, in which the highly cross-linked gel products grow in size until they are large enough to precipitate out of the suspension [9,10]. Normally, the aluminosilicate gel has dark grey in back-scattered scanning electron microscope (BSEM) image while the fly ash/slag particles have light grey, which indicates that the aluminosilicate gel has a lower density than the raw materials [19,45]. Thus, it can be concluded that the aluminosilicate gel is a space-filling gel due to its higher volume than the original binder. However, the aluminosilicate gel would also reorganize and rearrange to a denser gel such as C-A-S-H gel [55]. This denser packing process

would result in the collapse of gel pores and refinement of pore structure and finally may lead to autogenous shrinkage [57]. It is indicated that the reorganization and rearrangement of aluminosilicate gel structure would also likely contribute to the development of autogenous shrinkage of AAFS pastes in hardened stage.

The autogenous shrinkage fractions of AAFS pastes in different stages are plotted in Fig. 15 to further identify the shrinkage mechanism. The largest autogenous shrinkage fraction of AAFS pastes occurs in liquid stage (68.41%–72.57%), followed by hardened stage (17.65%–20.37%) and transition stage (6.86%–11.22%). It indicates that the chemical shrinkage mainly contributes to the autogenous shrinkage of AAFS pastes (around 70% of total autogenous shrinkage) at first 24 h after casting.

5. Conclusions

In this study, the early-age autogenous shrinkage of AAFS pastes with different slag content was investigated. Based on the experimental results, the main conclusions can be drawn as follows:

- The development of autogenous shrinkage generally follows the similar trends but different magnitudes for all the mixtures, in which AAFS pastes with higher slag content exhibit a higher magnitude since the addition of slag would accelerate the chemical reaction process.
- The autogenous shrinkage of AAFS pastes in liquid stage (from 0 h to initial setting time) is mainly attributed to volume contraction by chemical shrinkage, which arises from the absolute volume reduction of reaction products comparing with the original volume of unreacted binder. This phenomenon is similar to that found in PC systems.
- The ultimate autogenous shrinkage of AAFS paste with 10% slag (i.e., FS10) is lower than that of AAFS paste with 30% slag (i.e., FS30). However, the volume fraction of small pores of FS10 (31.79%) that is related to self-desiccation resulting from a decrease in internal RH is much higher than that of FS30 (9.60%). In addition, the internal RH evolution of all AAFS pastes during the early 24 h is almost the same. It indicates that the autogenous shrinkage of AAFS pastes may be not fully attributed to self-desiccation in hardened state. Some other mechanisms including the continuous reorganization and rearrangement of aluminosilicate gel structure may also contribute to autogenous shrinkage.

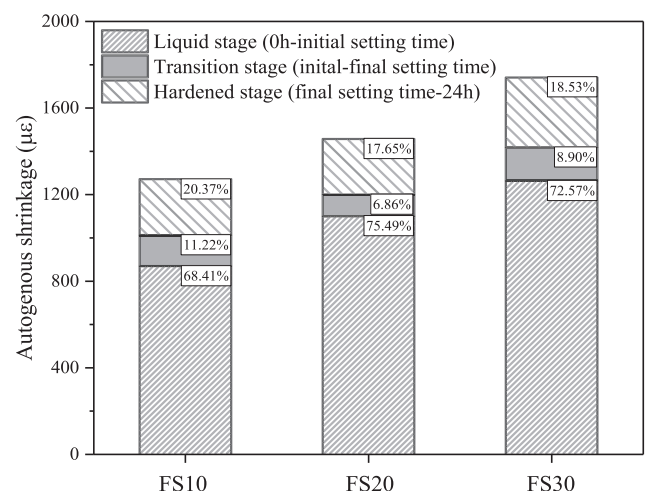


Fig. 15. Autogenous shrinkage fractions of AAFS pastes with different slag content at different stages.

- The autogenous shrinkage of AAFS pastes at first 24 h after casting occurs mainly due to volume contraction by chemical shrinkage in fresh state, which occupies approximately 70% of total autogenous shrinkage.

Conflict of interest

None.

Acknowledgements

The authors gratefully acknowledge the financial support of the Royal Society (IE150587) and EPSRC (EP/R041504/1). The financial support provided by University College London (UCL) and China Scholarship Council (CSC) to the first author is gratefully acknowledged. The authors would like to thank Dr Sam Ghazizadeh, Mr Min Liu, Mrs Shuqiong Luo, Mr Bin Zhang, Mr Chun Wai Goh and Miss Wenlin Tu for their support throughout this research. The authors would also like to thank Mr Warren Gaynor and Dr Shi Shi from UCL Laboratory of Advanced Materials and Dr Judith Zhou from UCL Environmental Engineering Laboratory for their help with experiments.

References

- [1] J.L. Provis, Alkali-activated materials, *Cem. Concr. Res.* (2017).
- [2] J.L. Provis, A. Palomo, C. Shi, Advances in understanding alkali-activated materials, *Cem. Concr. Res.* 78 (2015) 110–125.
- [3] C. Shi, A.F. Jiménez, A. Palomo, New cements for the 21st century: the pursuit of an alternative to Portland cement, *Cem. Concr. Res.* 41 (2011) 750–763.
- [4] F. Pacheco-Torgal, J.A. Labrincha, C. Leonelli, A. Palomo, P. Chindaprasirt, *Handbook of Alkali-activated Cements, Mortars and Concretes*, Woodhead Publishing, 2014.
- [5] M. Palacios, P.F.G. Banfill, F. Puertas, Rheology and setting of alkali-activated slag pastes and mortars: effect of organic admixture, *ACI Mater. J.* 105 (2008) 140–148.
- [6] Y. Fan, S. Yin, Z. Wen, J. Zhong, Activation of fly ash and its effects on cement properties, *Cem. Concr. Res.* 29 (1999) 467–472.
- [7] K. Somna, C. Jaturapitakkul, P. Kajitvichyanukul, P. Chindaprasirt, NaOH-activated ground fly ash geopolymer cured at ambient temperature, *Fuel* 90 (2011) 2118–2124.
- [8] F. Puertas, S. Martínez-Ramírez, S. Alonso, T. Vázquez, Alkali-activated fly ash/slag cements: strength behaviour and hydration products, *Cem. Concr. Res.* 30 (2000) 1625–1632.
- [9] I. Ismail, S.A. Bernal, J.L. Provis, R. San Nicolas, S. Hamdan, J.S.J. van Deventer, Modification of phase evolution in alkali-activated blast furnace slag by the incorporation of fly ash, *Cem. Concr. Compos.* 45 (2014) 125–135.
- [10] S.A. Bernal, J.L. Provis, B. Walkley, R. San Nicolas, J.D. Gehman, D.G. Brice, A.R. Kilcullen, P. Duxson, J.S.J. van Deventer, Gel nanostructure in alkali-activated binders based on slag and fly ash, and effects of accelerated carbonation, *Cem. Concr. Res.* 53 (2013) 127–144.
- [11] P. Nath, P.K. Sarker, Effect of GGBFS on setting, workability and early strength properties of fly ash geopolymer concrete cured in ambient condition, *Constr. Build. Mater.* 66 (2014) 163–171.
- [12] K. Parthiban, K. Saravananarajamohan, S. Shobana, A.A. Bhaskar, Effect of replacement of slag on the mechanical properties of fly ash based geopolymer concrete, *Int. J. Eng. Technol.* 5 (2013) 2555–2559.
- [13] P.S. Deb, P. Nath, P.K. Sarker, The effects of ground granulated blast-furnace slag blending with fly ash and activator content on the workability and strength properties of geopolymer concrete cured at ambient temperature, *Mater. Des.* 62 (2014) 32–39.
- [14] W.-C. Wang, H.-Y. Wang, M.-H. Lo, The fresh and engineering properties of alkali activated slag as a function of fly ash replacement and alkali concentration, *Constr. Build. Mater.* 84 (2015) 224–229.
- [15] G. Fang, W.K. Ho, W. Tu, M. Zhang, Workability and mechanical properties of alkali-activated fly ash-slag concrete cured at ambient temperature, *Construction and Building Materials*, under revision.
- [16] X. Fan, M. Zhang, Behaviour of inorganic polymer concrete columns reinforced with basalt FRP bars under eccentric compression: an experimental study, *Compos. B Eng.* 104 (2016) 44–56.
- [17] X. Fan, M. Zhang, Experimental study on flexural behaviour of inorganic polymer concrete beams reinforced with basalt rebar, *Compos. B Eng.* 93 (2016) 174–183.
- [18] P.S. Deb, P. Nath, P.K. Sarker, Drying shrinkage of slag blended fly ash geopolymer concrete cured at room temperature, *Procedia Eng.* 125 (2015) 594–600.
- [19] N.K. Lee, J.G. Jang, H.K. Lee, Shrinkage characteristics of alkali-activated fly ash/slag paste and mortar at early ages, *Cem. Concr. Compos.* 53 (2014) 239–248.
- [20] J.J. Brooks, 6 – Shrinkage of Concrete, Butterworth-Heinemann, Concrete and Masonry Movements, 2015, pp. 137–185.
- [21] Y. Ma, G. Ye, The shrinkage of alkali activated fly ash, *Cem. Concr. Res.* 68 (2015) 75–82.
- [22] F. Collins, J.G. Sanjayan, Effect of pore size distribution on drying shrinkage of alkali-activated slag concrete, *Cem. Concr. Res.* 30 (2000) 1401–1406.
- [23] R.J. Thomas, D. Lezama, S. Peethamparan, On drying shrinkage in alkali-activated concrete: Improving dimensional stability by aging or heat-curing, *Cem. Concr. Res.* 91 (2017) 13–23.
- [24] A.A. Melo Neto, M.A. Cincotto, W. Repette, Drying and autogenous shrinkage of pastes and mortars with activated slag cement, *Cem. Concr. Res.* 38 (2008) 565–574.
- [25] M.O. Yusuf, M.A. Megat Johari, Z.A. Ahmad, M. Maslehuddin, Shrinkage and strength of alkaline activated ground steel slag/ultrafine palm oil fuel ash pastes and mortars, *Mater. Des.* 63 (2014) 710–718.
- [26] C. Duran Atiş, C. Bilim, Ö. Çelik, O. Karahan, Influence of activator on the strength and drying shrinkage of alkali-activated slag mortar, *Constr. Build. Mater.* 23 (2009) 548–555.
- [27] T. Bakharev, J.G. Sanjayan, Y.B. Cheng, Effect of elevated temperature curing on properties of alkali-activated slag concrete, *Cem. Concr. Res.* 29 (1999) 1619–1625.
- [28] M. Hojati, A. Radlińska, Shrinkage and strength development of alkali-activated fly ash-slag binary cements, *Constr. Build. Mater.* 150 (2017) 808–816.
- [29] D. Hou, H. Ma, Y. Zhu, Z. Li, Calcium silicate hydrate from dry to saturated state: Structure, dynamics and mechanical properties, *Acta Mater.* 67 (2014) 81–94.
- [30] D. Hou, H. Ma, Z. Li, Z. Jin, Molecular simulation of “hydrolytic weakening”: a case study on silica, *Acta Mater.* 80 (2014) 264–277.
- [31] P. Lura, O.M. Jensen, K. Van Breugel, Autogenous shrinkage in high-performance cement paste: an evaluation of basic mechanisms, *Cem. Concr. Res.* 33 (2003) 223–232.
- [32] Z. Jiang, Z. Sun, P. Wang, Autogenous relative humidity change and autogenous shrinkage of high-performance cement pastes, *Cem. Concr. Res.* 35 (2005) 1539–1545.
- [33] J.J. Thomas, H.M. Jennings, A colloidal interpretation of chemical aging of the C-S-H gel and its effects on the properties of cement paste, *Cem. Concr. Res.* 36 (2006) 30–38.
- [34] I. Garcia-Lodeiro, A. Palomo, A. Fernández-Jiménez, D.E. Macphee, Compatibility studies between N-A-S-H and C-A-S-H gels. Study in the ternary diagram $\text{Na}_2\text{O}-\text{CaO}-\text{Al}_2\text{O}_3-\text{SiO}_2-\text{H}_2\text{O}$, *Cem. Concr. Res.* 41 (2011) 923–931.
- [35] N.K. Lee, H.K. Lee, Reactivity and reaction products of alkali-activated, fly ash/slag paste, *Constr. Build. Mater.* 81 (2015) 303–312.
- [36] J.G. Jang, N.K. Lee, H.K. Lee, Fresh and hardened properties of alkali-activated fly ash/slag pastes with superplasticizers, *Constr. Build. Mater.* 50 (2014) 169–176.
- [37] E. Holt, Contribution of mixture design to chemical and autogenous shrinkage of concrete at early ages, *Cem. Concr. Res.* 35 (2005) 464–472.
- [38] M.N. Amin, J.-S. Kim, T.T. Dat, J.-K. Kim, Improving test methods to measure early age autogenous shrinkage in concrete based on air cooling, *IES J. Part A: Civ. Struct. Eng.* 3 (2010) 244–256.
- [39] P. Turcay, A. Loukili, Evaluation of plastic shrinkage cracking of self-consolidating concrete, *Mater. J.* 103 (2006) 272–279.
- [40] ASTM C1608-12, Standard test method for chemical shrinkage of hydraulic cement paste, ASTM International, West Conshohocken, PA, 2012.
- [41] ASTM C230-14, Standard specification for flow table for use in tests of hydraulic cement, ASTM International, West Conshohocken, PA, 2014.
- [42] ASTM C191-13, Standard test methods for time of setting of hydraulic cement by vicat needle, ASTM International, West Conshohocken, PA, 2013.
- [43] H. Ma, Mercury intrusion porosimetry in concrete technology: tips in measurement, pore structure parameter acquisition and application, *J. Porous Mater.* 21 (2014) 207–215.
- [44] J. Kaufmann, R. Loser, A. Leemann, Analysis of cement-bonded materials by multi-cycle mercury intrusion and nitrogen sorption, *J. Colloid Interface Sci.* 336 (2009) 730–737.
- [45] H. Ye, A. Radlińska, Fly ash-slag interaction during alkaline activation: Influence of activators on phase assemblage and microstructure formation, *Constr. Build. Mater.* 122 (2016) 594–606.
- [46] S. Puligilla, P. Mondal, Role of slag in microstructural development and hardening of fly ash-slag geopolymer, *Cem. Concr. Res.* 43 (2013) 70–80.
- [47] S. Chithiraputhiran, N. Neithalath, Isothermal reaction kinetics and temperature dependence of alkali activation of slag, fly ash and their blends, *Constr. Build. Mater.* 45 (2013) 233–242.
- [48] B. Singh, M.R. Rahman, R. Paswan, S.K. Bhattacharyya, Effect of activator concentration on the strength, ITZ and drying shrinkage of fly ash/slag geopolymer concrete, *Constr. Build. Mater.* 118 (2016) 171–179.
- [49] S.M. Park, J.G. Jang, N.K. Lee, H.K. Lee, Physicochemical properties of binder gel in alkali-activated fly ash/slag exposed to high temperatures, *Cem. Concr. Res.* 89 (2016) 72–79.
- [50] IUPAC, Manual of symbols and terminology for physicochemical quantities and units, appendix 2, part 2, Colloid and Surface Chemistry, International Union of Pure and Applied Chemistry, 1976.
- [51] P. Mounanga, M. Bouasker, A. Pertue, A. Perronnet, A. Khelidj, Early-age autogenous cracking of cementitious matrices: physico-chemical analysis and micro/macro investigations, *Mater. Struct.* 44 (2011) 749–772.

- [52] E.-I. Tazawa, S. Miyazawa, T. Kasai, Chemical shrinkage and autogenous shrinkage of hydrating cement paste, *Cem. Concr. Res.* 25 (1995) 288–292.
- [53] V. Šmilauer, P. Hlaváček, F. Škvára, R. Šulc, L. Kopecký, J. Němeček, Micromechanical multiscale model for alkali activation of fly ash and metakaolin, *J. Mater. Sci.* 46 (2011) 6545–6555.
- [54] C.J. Brinker, G.W. Scherer, *Sol-Gel Science: The Physics and Chemistry of Sol-gel Processing*, Academic Press, INC, 1990.
- [55] I. García-Lodeiro, A. Fernández-Jiménez, A. Palomo, Variation in hybrid cements over time. Alkaline activation of fly ash-portland cement blends, *Cem. Concr. Res.* 52 (2013) 112–122.
- [56] G.W. Scherer, Structure and properties of gels, *Cem. Concr. Res.* 29 (1999) 1149–1157.
- [57] H. Ye, A. Radlińska, Shrinkage mechanisms of alkali-activated slag, *Cem. Concr. Res.* 88 (2016) 126–135.